Chemical Geology 393–394 (2015) 112–124

Contents lists available at ScienceDirect

Chemical Geology

journal homepage: www.elsevier.com/locate/chemgeo

Magnesium isotope composition of sabkha porewater and related (Sub-) Recent stoichiometric dolomites, Abu Dhabi (UAE)

A. Geske [a,*], S. Lokier [b], M. Dietzel [c], D.K. Richter [a], D. Buhl [a], A. Immenhauser [a]

[a] Ruhr-University Bochum, Institute for Geology, Mineralogy and Geophysics, Universitätsstraße 150, D-44801 Bochum, Germany
[b] Petroleum Geosciences Department, The Petroleum Institute, P.O. Box 2533, Abu Dhabi, United Arab Emirates
[c] Institute of Applied Geosciences, Graz University of Technology, 8010 Graz, Austria

ARTICLE INFO

Article history:
Received 8 August 2014
Received in revised form 17 November 2014
Accepted 18 November 2014
Available online 27 November 2014

Editor: Michael E. Böttcher

Keywords:
Magnesium isotopes
Holocene sabkha dolomites
Isotope fractionation
Low temperature dolomitization

ABSTRACT

Earliest marine diagenetic sabkha type dolomites are widespread in Earth's geological record. Potentially, these carbonates may act as archives of past seawater magnesium isotope ($\delta^{26}Mg$) ratios. At present, however, the fractionation of magnesium isotopes ($\Delta^{26}Mg$) between seawater – here evaporated marine porewater – and sabkha dolomite is not constrained. In order to explore $\Delta^{26}Mg_{dol\text{-}Mg(porewater)}$, we make use of actualistic sabkha type dolomite precipitation in the Gulf region (Trucial coast, United Arab Emirates). This paper documents and discusses the first detailed sabkha $\delta^{26}Mg$ data set of Mg-bearing solids including stoichiometric dolomites (degree of ordering >0.9; mean $\delta^{26}Mg_{dol} = -0.79‰ \pm 0.41$ 2σ, n = 17) and related marine pore waters. The presence of dolomite crystals with a broad range of ordering in shallow cores is documented using X-ray diffraction and scanning electron microscopy, but individual crystals are too small (<10 μm) to be mechanically separated from their host sediment. Hence, a method was developed to chemically separate the most stoichiometric dolomite crystals from coexisting less stoichiometric dolomites and other Mg-bearing minerals and fluid phases by using disodium ethylenediaminetetracetic acid. Sabkha shallow ground water collected in trenches displays $\delta^{26}Mg$ values of about −0.59‰, i.e. is only moderately enriched in ^{26}Mg relative to the present-day seawater signature of −0.83‰. Conversely, the $\delta^{26}Mg$ of evaporated porewater is enriched by +0.43‰ relative to that of $\delta^{26}Mg_{seawater}$. Here we use the term "apparent" fractionation for the variable $\Delta^{26}Mg_{dol\text{-}Mg(porewater)}$ (+0.1 and −0.7‰) obtained that cannot be compared with experimentally deduced fractionation factors from controlled laboratory settings. Moreover, evaporated sabkha porewater differs, in terms of its isotope signature, from seawater. With regard to the current level of knowledge, the hypothesis that earliest diagenetic sabkha dolomites represent direct archives of secular changes of seawater $\delta^{26}Mg$ values with time is not supported by our dataset. Our present understanding is that the magnesium isotope signature of sabkha dolomites is related to complex kinetics of precursor formation, dissolution/precipitation reactions including microbiological effects and involves variable Mg sources and sinks in a temporally and spatially variable microenvironment.

1. Introduction

Magnesium is a main component of dolomite and a minor element in many carbonates (Warren, 2000). In marine settings, the main source of Mg for dolomite formation is seawater. Consequently, the Mg concentration and the $\delta^{26}Mg$ isotopic composition of seawater and of marine porewaters are of particular interest. Modern seawater $\delta^{26}Mg$ values are in the order of −0.83‰ independent of water depth or geographic location (see references in Hippler et al., 2009) and long $Mg_{seawater}$ residence times of τ ~ 13 Myr were suggested by Broecker and Peng (1982).

These considerations form a strong motivation to explore earliest diagenetic (marine porewater/sabkha) dolomites as archives of secular changes in past seawater $\delta^{26}Mg$ values. Nevertheless, this approach is severely hampered by the, at present, poorly constrained dolomite-aqueous Mg isotope fractionation factor. This factor, and the difference between seawater and evaporated sabkha porewater $\delta^{26}Mg$, is required to hindcast past seawater magnesium isotope ratios from fossil sabkha dolomites. Sabkha-type, non-stoichiometric dolomites have received considerable attention as bacterial sulfate reduction and methanogens trigger the dolomitization process (Hardie, 1987; Compton, 1988; Wright, 1997; Vasconcelos et al., 1995; Vasconcelos and McKenzie, 1997; Mazzullo, 2000; Warthmann et al., 2000; Van Lith et al., 2002, 2003a, 2003b; Roberts et al., 2004, 2013; Wright and Wacey, 2005; Sánchez-Román et al., 2008, 2009, 2011; Kenward et al., 2009; Deng et al., 2010; Bontognali et al., 2010). Previous research indicates a

* Corresponding author. Tel.: +49 234 3225457.
E-mail address: Anna.Geske@rub.de (A. Geske).

http://dx.doi.org/10.1016/j.chemgeo.2014.11.020
0009-2541/

significant depletion of modern microbial dolomite δ^{26}Mg by up to 2–3‰ relative to the water from which it is formed (Carder et al., 2005) but the obtained $\Delta^{26}Mg_{dol\text{-}Mg(aq)}$ values do not discriminate between equilibrium and kinetic effects.

Azmy et al. (2013) reported that the Mg isotopic fractionation between seawater and bulk sabkha sediment is minor (Δ^{26}Mg = +0.22‰). These authors analyzed dolomite-bearing sabkha bulk sediments containing a variety of Mg-bearing phases (such as 22–32 wt.% calcite and 47–55 wt.% anhydrite) along with dolomite, which is one of the volumetrically least important phases (~10 wt.%). In a comprehensive study, Higgins and Schrag (2010) analyzed porewater and authigenic dolomites in several ODP cores (Upper Miocene to Upper Pleistocene). These authors found that the Mg isotope values of the authigenic dolomites are depleted by 2 to 2.7‰ relative to the porewater. While the work of Higgins and Schrag (2010) is at present the most rigorous and quantitative approach dealing with magnesium isotope fractionation in Neogene early diagenetic dolomites, two important questions remain open: (i) is the present-day porewater in the Neogene cores representative for the original porewater from which these dolomites precipitated and (ii) is the presently measured δ^{26}Mg of these fossil dolomites representative of the pristine values at precipitation?

This paper presents a comprehensive δ^{26}Mg data set of modern seawater, sabkha shallow ground water, sabkha porewater and related stoichiometric dolomites from short cores taken in the modern Abu Dhabi (Lokier and Steuber, 2008) sabkha environment. The data set also includes δ^{26}Mg ratios of all other volumetrically significant Mg bearing mineral phases (calcite and gypsum) as well as data from organic material in microbial mats. We here aim to (i) establish a protocol for the extraction and analysis of volumetrically subordinate, 5–10 μm-sized stoichiometric dolomite crystals from a Mg-phase-rich host sediment; (ii) to assess the apparent Mg isotope fractionation between stoichiometric dolomites, their corresponding porewater, and local sea water and, finally, (iii) to decipher potential trends of δ^{26}Mg values as a function of profile depth.

2. Geological setting

2.1. Sampling sites

The sampling sites are located on the Persian Gulf shoreline of the United Arab Emirates (UAE) about 50 km south-west of Abu Dhabi Island. The four representative locations are referred to Site 1a (rSD1a) (24 07.016 N; 54 03.229 E), Site 1b (rSD1b) (24 07.025 N; 54 03.171 E), Site 3 (rSD3) (24 07.051 N; 54 02.994 E) and Site 5 (rSD5) (24 07.087 N; 54 02.759 E; Fig. 1; Lokier and Steuber, 2008). The upper intertidal zone is characterized by living microbial mats (Butler, 1969). Tidal flat mud core from Sites 1b (rSD1b) and 3 (rSD3), investigated in this study, are located in the upper intertidal zone of the sabkha (Fig. 1). Absolute altitudes of sabkha cores are approximately 2.8 m (rSD1b) and 2.7 m (rSD3) above sea level. Samples were taken from seawater, lagoon water (24 30.820 N; 54 23.483 E); (24 09.306 N; 54 04.642 E) and shallow groundwater draining the sabkha (24 08.045 N; 54 05.565 E).

The southern coast of the Persian Gulf is a low-angle ramp (0.4 m/km) composed of Holocene carbonate and evaporite sediments that unconformably overlie Pleistocene carbonate-rich sandstones and Paleogene/Neogene bedrock (Evans et al., 1969). Flandrian sea-level rise peaked between 4000 and 6000 years BP at a height 1–2 m above today's sea level (Evans et al., 1969; Kinsman, 1969; Patterson and Kinsman, 1977). The resulting interbedded carbonate and clastic transgressive sediments exhibit an upwards-fining trend and reach up to 3 m in thickness (Evans et al., 1969). This flooding event removed the source of sand to the southern Gulf shoreline, thus promoting deflation of the coastal land surface to the level of the water table. Sabkhas began to form along the present coastline at ~4000 years BP (Evans et al., 1969; Kinsman, 1969). Sampling sites are located in the upper intertidal zone of the sabkha and the oldest radiocarbon ages of the investigated tidal flat cores vary between 1441 and 786 years cal BP (Lokier and Steuber, 2008).

The earliest diagenetic sabkha (non-stoichiometric) dolomites precipitated from evaporated porewater in microbial mats within the

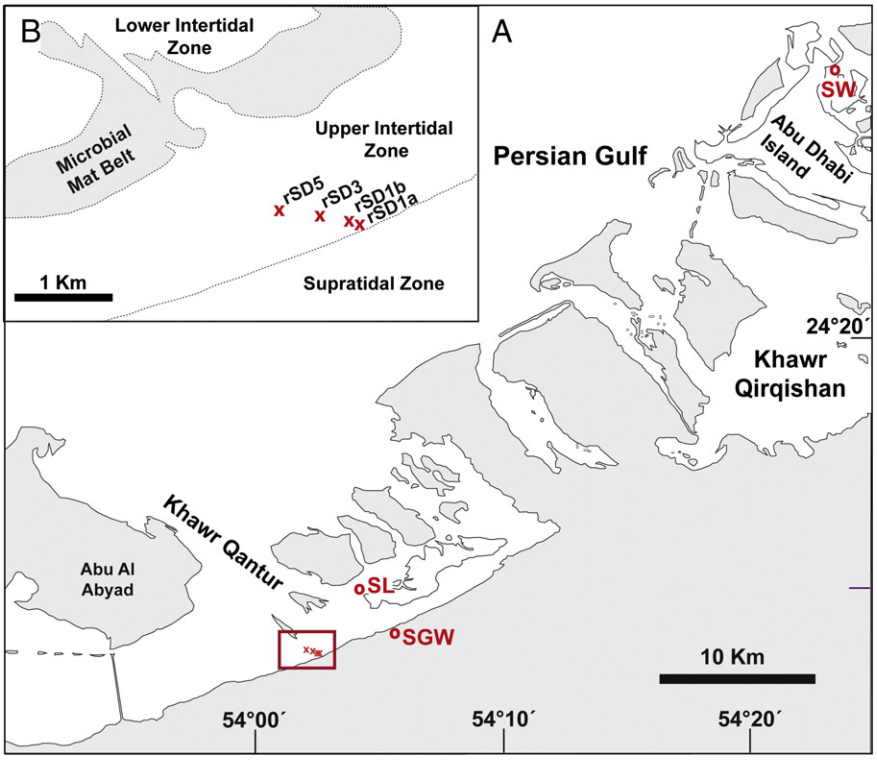

Fig. 1. A) Map of the United Arab Emirates coastline between Abu Dhabi and Abu Al Abyad islands showing the location of the study area and localities where water samples were taken (SL = lagoon water; SGW = groundwater; SW = seawater). B) Map of the study area showing the location of the sampling sites.
The two maps are modified after Lokier and Steuber (2008).

sediment in less than one meter depth at fluid temperatures between 34 and 49 °C (McKenzie et al., 1980; Lokier, 2012). Their recent to sub-recent age was determined with radiocarbon dating (Illing et al., 1965; Evans et al., 1969; Patterson and Kinsman, 1977; Purser et al., 1994; Lokier and Steuber, 2008).

2.2. Climate/hydrology

The climate of the studied sabkha is arid with an annual air temperature between 7 and 50 °C. Temperatures within the sediment, 25 cm below the sabkha surface, reach up to 43 °C during the summer, with a diurnal range of only 4 °C, and 17 °C during the winter with a diurnal range of 0.3 °C (Lokier, 2012). The combination of strong winds, high temperature and low rainfall (average: 72 mm/a) results in elevated evaporation rates, high salinities and accordingly in precipitation of evaporite minerals including halite, anhydrite and/or gypsum. Net evaporation yields in elevated salinities of 45–46 g/l along the open-marine coast of Abu Dhabi and up to 89 g/l in more-restricted lagoons (Lokier and Steuber, 2009). Water temperatures vary from 23 to 24 °C and in the nearshore from 22 to 36 °C in the inner lagoon (Evans et al., 1969).

The dynamic movement of the highly saline porewater in the sediment is controlled by two main processes: (i) evaporative pumping inducing an upward flow of the porewater and (ii) recharge by seawater flooding rejuvenates older interstitial brines by downward soaking (Baltzer et al., 1994).

3. Material and methods

3.1. Sampling techniques and sample description

Percussion cores were taken inserting a polycarbonate tube into the sabkha surface and then digging a hole immediately adjacent to the core tube in order to recover the core without any loss of material. In this way it was possible to assess the degree of coring-induced compaction which was deemed to be negligible. Cores were immediately marked for orientation and capped in order to retain porewater. Porewater was collected by digging a pit to intersect the water table and inserting a 20 cm long perforated tube into the wall of the pit at a depth of 1 m.

3.1.1. Facies types

The main facies types are unconsolidated to weakly cemented carbonate sediments, which vary laterally and vertically between bioclastic sands to micritic muds containing isolated bioclasts (Lokier and Steuber, 2008). The carbonate horizon of tidal mud core rSD3 is overlain by buried laminated microbial mats and the sediment surface is dominated by evaporites (Fig. 2). Tidal flat core rSD1b shows an inverse pattern. Here carbonate mud with sand and fossils overlies a reworked, less-laminated microbial mat facies. Evaporite sediment layers above the microbial mat are lacking.

3.2. Sample treatment

Tidal flat cores within plastic tubes were exposed to dry ice for 12 h prior to cutting, in order to freeze the highly saline porewater. Subsequently, cores were cut longitudinally with a band saw into one cm-thick slices. One half of the core was preserved as repository material, the other half was used for further treatment. Cores were kept frozen at −30 °C until processing. Target sampling intervals for dolomites are dark brown layers (microbial mat facies) and grayish sediment (carbonate mud with gypsum; black arrows in Fig. 2). Prior to mineralogical and geochemical analyses, samples were washed with deionized H_2O (>18.2 MΩ cm^{-1}) in order to remove highly soluble salts such as sodium chloride, potassium chloride, magnesium chloride and gypsum and to avoid artifact precipitation of salt minerals. Subsequently, samples were dried in an oven at 40 °C. Carbonate bioclasts and larger anhydrite/gypsum crystals were separated manually from the bulk sediment and the remaining bulk sediment was pestled. The sediment samples were centrifuged and the water was pipetted.

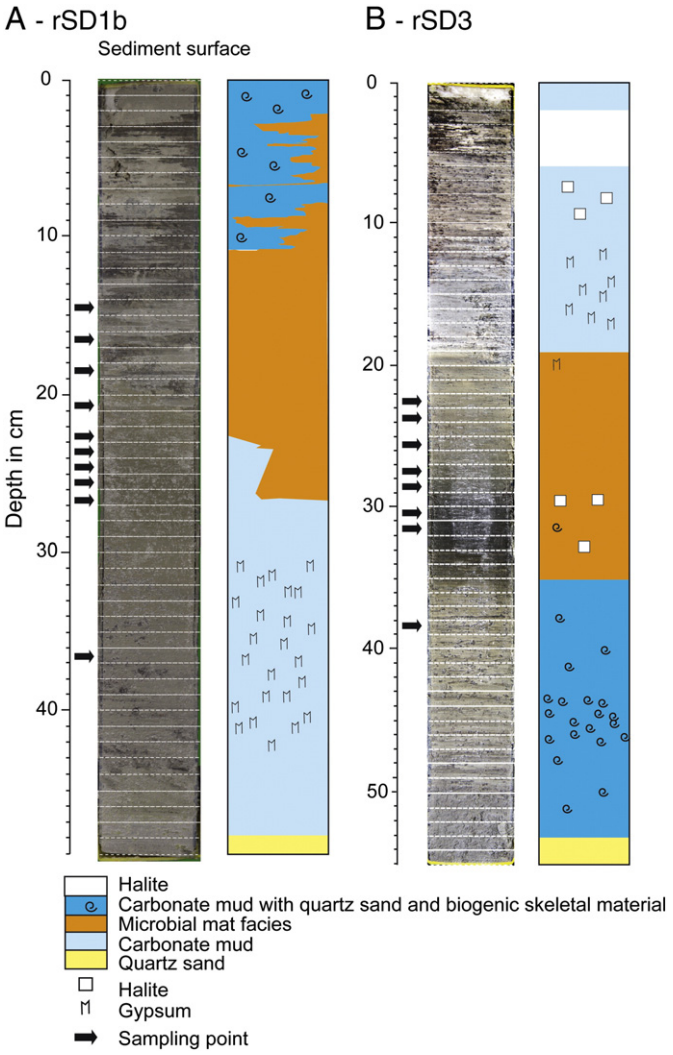

Fig. 2. Sampled sedimentary logs of A) Site 1 (rSD1b) and B) Site 3 (rSD3) showing the facies types/carbonate mineralogy correlated to sediment depth in centimeter. Sampling points are marked by black arrows. Site locations are indicated in Fig. 1.

3.2.1. Crystallographic analysis

An emulsion of sample and deionized water was pipetted on a glass sample plate and was dried at 40 °C. Organic matter from microbial mats was removed by bleaching with hydrogen peroxide. In addition pre-treated powdered aliquots were measured to confirm the applicability of the EDTA Method on sabkha dolomites. The mineralogy of the sediments was determined with a Phillips X'Pert MPD Theta-Theta X-Ray Diffractometer at the Ruhr-University Bochum, Germany. The X-ray source is a long-fine-focus, ceramic X-ray tube with a Cu anode producing Cu Kα wavelength of 1.5405 Å. The measurement conditions include high voltage of 45 kV, a current of 40 mA, an angular range from 2 to 65, a step size of 0.035 °2θ and a counting time of 20 s. A graphite secondary monochromator was used to minimize the background noise.

3.2.2. Scanning electron microscopy

Scanning electron microscopy (SEM) was performed with a high resolution thermally aided Field Emission SEM 1530 Gemini FESEM by LEO (Zeiss) equipped with an INCA X-ray microanalysis system. Aliquots were dried at room temperature and fresh surfaces were obtained by breaking the samples (cold fracture). The samples were spotted with gold (Au peaks). Images and energy dispersive X-ray spectroscopy

(EDX) analyses were obtained with a backscatter detector at an accelerating voltage of 20 kV and a working distance of 13 mm.

3.2.3. Magnesium isotope analysis ($\delta^{26}Mg$)

A 500 ppb Mg-solution in 3.5% HNO_3 was measured on a Thermo Fisher Scientific Neptune MC-ICP-MS. The difference between the Mg concentration of the standard and sample was kept within a 15% limit, which proved minimizing potential isobaric interferences from matrices (Galy et al., 2001). A positive effect on signal stability and reduction of matrix interferences was achieved by combining two desolvating systems, ApexIR (ESI) and Aridus (Cetac) and the low-resolution slit of the Thermo Fisher Scientific Neptune. The standard sample bracketing technique was applied to calculate the $\delta^{25}Mg$ and $\delta^{26}Mg$ values (‰). The reproducibility of Mg isotope measurements was assessed using samples of i) the internal carbonate standard RUB (Solnhofen Plattenkalk), ii) the mono elemental solution Cambridge1, iii) IAPSO seawater and iv) a dolomite sample (HDK7). The 2σ external reproducibility ($\delta^{26}Mg_{DSM3}$) for these (standard) materials is: −2.02 ± 0.02‰ (Dolomite HDK7, n = 5), −3.66 ± 0.06‰ (RUB limestone, n = 5), −0.81 ± 0.06‰ (IAPSO seawater, n = 130), −2.58 ± 0.07‰ (Cambridge I, n = 519). The latter results are indistinguishable from published values ($\delta^{25}Mg_{Cambridge1} = -2.58 \pm 0.14$‰ 2σ, n = 35; Galy et al., 2003; Young and Galy, 2004). The total blank for the complete analysis was 10 ng Mg, which represents an average blank-to-sample ratio of $2 * 10^{-4}$. For further details on the analytical methods please refer to the digital Appendix and to Geske et al. (2012).

3.2.4. Elemental analysis

Approximately 1.5 mg of the dolomite samples were dissolved in 3 M HNO_3. Afterwards the solution was diluted with 2 ml of deionized H_2O (>18.2 MΩ cm^{-1}). With an inductively coupled plasma optical emission spectrometer (ICP-OES, Thermo Fisher Scientific iCAP 6500 DUO) the concentration of Ca, Mg, Fe, Mn, Sr and Ba of the carbonate samples were measured at the Ruhr-University Bochum. With each set of samples, eight samples of certified reference material (BSC-CRM-512, dolomite and BSC-CRM-513, limestone) were analyzed. All major and trace element concentrations are reported in ppm (parts per million). Analytical errors are given as ±%RSD. The 1σ-reproducibility for the major- and trace elements of the two standard materials is: ±0.18% for Ca, ±0.081% for Mg, ±22 ppm for Sr, ±17 ppm for Fe and ±1 ppm for Mn (CRM-512, n = 111) and ±0.36% for Ca ±0.002% for Mg, ±1 ppm for Sr, ±12 ppm for Fe and ±1 ppm for Mn (CRM-513, n = 111).

4. Separation of stoichiometric dolomite from its host sediment

The separation and extraction of volumetrically insignificant, submillimeter stoichiometric dolomite crystals from unconsolidated sabkha sediment, composed of a complex array of carbonate, sulfate, chloride and silicate minerals and a highly concentrated Mg and Na chloride porewater, is exceptionally challenging. The approach developed in the present study leads to a sequential removal of interfering Mg-bearing mineral phases and the separation and purification of dolomite crystals. This approach does not separate the metastable, non-stoichiometric dolomites and corresponding highest-Mg phases that do not qualify as dolomites. A detailed description of the protocol is documented in the digital Appendix. The approach used here is based on the work of Babcock et al. (1967) making use of the differential etching properties of calcite and dolomite applying diluted (0.27 M) disodium ethylenediaminetetracetic acid (di-Na-EDTA) solution at pH 6.3 (Glover, 1961) without dissolving other minerals. Di-Na-EDTA is a strongly chelating agent for metal ions with a charge >2+. With respect to carbonate minerals the dissolution/etching order of EDTA is calcite < aragonite < non-stoichiometric dolomite < stoichiometric dolomite < magnesite, whereby calcite is the most susceptible and magnesite is the least susceptible to EDTA treatment (Bodine and Fernalld, 1973). Samples containing magnesite (proved with X-ray diffraction-, and EDX measurements) were not used for Mg isotope analyses, to avoid an admixture of dolomite-magnesite end-products. The dissolution order is important, as only the most stoichiometric dolomites (degree of ordering >0.9) escape the dissolution procedure and were analyzed in the context of this study. The degree of order (R) of EDTA treated dolomite was calculated with the following equation:

$$R = I\ d_{(015)} / I\ d_{(110)}$$

whereby (I) is the intensity of the peaks (015) (superstructure peak) and (110) in counts per second (cps); Füchtbauer and Goldschmidt, 1965; Füchtbauer and Richter, 1988; Hardy and Tucker, 1988. The degree of order of dolomite phases in untreated sediment samples could not be defined. This because the superstructure peak $d_{(015)}$ in x-ray diffraction patterns was not resolved due to insufficient concentration of dolomite in the untreated samples.

Briefly, powdered pre-treated samples were incinerated at 250 °C for 24 h to decompose organic components and aliquots were treated with 0.27 M di-Na-EDTA at pH 6.3 to separate the dolomite from coexisting calcite, Mg-calcite and aragonite (Fig. A6A and B; see Appendix). The remaining sediment was filtered through Teflon filter (pore size: 0.45 μm) and washed with deionized water to remove the di-Na-EDTA and organic components (ash) and dried at 40 °C. The remaining sediment sample containing dolomite and (Mg-bearing) clay minerals was dissolved in 1 M acetic acid for three days. The clay minerals that remained unchanged/undissolved (Ostrom, 1961) and potentially added Mg ions previously attached to their surface (exchangeable Mg) to the sample is negligible as this species was essentially removed by the pre-treatment with Na-ETDA. This was confirmed by analyzing $\delta^{26}Mg$ of sub-samples that were a) leached with 0.1 M acetic acid and b) not leached with acetic acid after EDTA treatment and by analyzing the clay residue of these samples (see Table A4). In contrast, the stoichiometric dolomite (>95 wt.%) was completely dissolved in acetic acid as proved by X-ray diffraction of the solid residue, which is composed only of clay minerals (Fig. A7 A, B; cf. Appendix).

5. Results

5.1. Mineralogy and microstructure

X-ray diffraction analyses indicate that the sabkha sediment, particularly the microbial mat facies, contain 7 to 14 wt.% of dolomite, 7 to 15 wt.% of calcite, 27 to 46 wt.% of aragonite, 3 to 14 wt.% of Mg-calcite, 5 to 14 wt.% of clay minerals (chlorite, muscovite/illite), 10 to 17 wt.% of albite, 8 to 14 wt.% of anhydrite/gypsum, about 10 wt.% of halite and 11 to 15 wt.% of quartz. Accordingly, dolomite was detected in all subsamples of tidal flat mud cores rSD1b and rSD3. Fig. A6A (see Appendix) documents the XRD pattern of a pre-treated sample. The separated dolomite is characterized by a main peak position at $d_{(104)} = 2.881–2.888$ corresponding to a $CaCO_3$ content ranging from 48 to 51 mol%. The dolomite superstructure peak $d_{(015)}$ was observed by X-ray pattern (Fig. A7B; digital Appendix) and indicates a high degree of ordering (0.95). Owing to the analytical procedure used here, the dolomites analyzed represent the ordered end-member of the total dolomite population in the Abu Dhabi sabkha (Table 1a).

SEM imaging of the microbial mat facies layers in the investigated cores show typically laminated microbial mats (Fig. 3a, see McKenzie and Vasconcelos, 2009; Last et al., 2012). Here, EDX analyses indicate an admixture of (phyllo-)silicates and halite. In the grayish carbonate mud (Fig. 2), dolomite, aragonite needles and magnesite were detected with EDX by their composition (Fig. 3b–d). Authigenic dolomite spheroids, with dimensions ranging from 10 to 20 μm, are distributed through the microbial mats (Fig. 4a, b, e, f). The spheroids are composed of rhombohedral dolomite crystals, each 1–2 μm in size (Fig. 4c). In the carbonate mud layers only rhombohedral dolomite has been found.

Table 1a
Magnesium isotopic composition of fluids and minerals within tidal flat mud cores rSD1b, rSD3 and water samples (dol = dolomite).

Material	Mineral	Facies	Sediment depth [cm]	δ^{25}Mg [‰DSM3]	±2σ	δ^{26}Mg [‰DSM3]	±2σ	Degree of order
Tidal flat mud core rSD1b								
Porewater		Microbial mat	11	−0.24	0.01	−0.46	0.01	
Porewater		Microbial mat	21	−0.22	0.01	−0.40	0.03	
Porewater		Carbonate mud	27	−0.23	0.01	−0.44	0.03	
Porewater		Gypsum mash	37	−0.25	0.01	−0.47	0.04	
$Porewater_{mean}$				−0.23	0.03	−0.44	0.06	
Solid	Bulk sediment	Microbial mat	20	−0.60	0.02	−1.14	0.01	
Solid	Gypsum	Gypsum mash	36	−0.53	0.01	−1.04	0.05	
Solid	Organics	Microbial mat	20	−0.44	0.02	−0.85	0.05	
Solid	Organics	Microbial mat	18	−0.37	0.02	−0.71	0.05	
Solid	Dol	Microbial mat	14	−0.46	0.03	−0.89	0.03	0.9
Solid	Dol	Microbial mat	16	−0.54	0.04	−1.05	0.05	0.9
Solid	Dol	Microbial mat	18	−0.57	0.03	−1.09	0.06	0.8
Solid	Dol	Microbial mat	20	−0.53	0.02	−1.04	0.04	0.9
Solid	Dol	Microbial mat	22	−0.44	0.03	−0.85	0.04	0.7
Solid	Dol	Microbial mat	23	−0.45	0.02	−0.87	0.03	0.9
Solid	Dol	Microbial mat	24	−0.40	0.03	−0.77	0.04	0.9
Solid	Dol	Carbonate mud	25	−0.43	0.01	−0.83	0.03	0.8
Solid	Dol	Carbonate mud	26	−0.41	0.02	−0.79	0.03	0.9
$Solid_{mean}$	Dol			−0.47	0.12	−0.91	0.24	
		Apparent $\Delta^{26}Mg_{Dol\text{-}Mg(Seawater)}$				−0.3 to +0.02		
		Apparent $\Delta^{26}Mg_{Dol\text{-}Mg(Porewater)}$				−0.3 to −0.7		
Tidal flat mud core rSD3								
Porewater		Carbonate mud	10	−0.27	0.03	−0.52	0.03	
Porewater		Microbial mat	20	−0.27	0.04	−0.52	0.04	
Porewater		Microbial mat	30	−0.27	0.03	−0.52	0.04	
Porewater		Carbonate mud	40	−0.23	0.02	−0.44	0.04	
Porewater		Carbonate mud	50	−0.12	0.01	−0.23	0.00	
$Porewater_{mean}$				−0.23	0.13	−0.45	0.25	
Solid	Bulk sediment	Microbial mat	25	−0.48	0.02	−0.94	0.04	
Solid	Gypsum	Gypsum mash	18	−0.51	0.03	−0.99	0.04	
Solid	Calcite	Microbial mat	31	−0.73	0.03	−1.40	0.04	
Solid	Dol	Microbial mat	22	−0.27	0.02	−0.52	0.04	0.8
Solid	Dol	Microbial mat	23	−0.27	0.02	−0.52	0.04	0.9
Solid	Dol	Microbial mat	25	−0.19	0.04	−0.38	0.07	0.9
Solid	Dol	Microbial mat	28	−0.32	0.02	−0.62	0.02	0.9
Solid	Dol	Microbial mat	30	−0.40	0.02	−0.77	0.04	0.8
Solid	Dol	Microbial mat	31	−0.45	0.02	−0.87	0.03	0.7
Solid	Dol	Carbonate mud	38	−0.49	0.02	−0.95	0.03	0.9
Solid	Dol	Microbial mat	27	−0.32	0.02	−0.61	0.04	0.9
$Solid_{mean}$	Dol			−0.34	0.21	−0.65	0.39	
		Apparent $\Delta^{26}Mg_{Dol\text{-}Mg(Seawater)}$				−0.16 to +0.41		
		Apparent $\Delta^{26}Mg_{Dol\text{-}Mg(Porewater)}$				−0.5 to +0.1		
Water samples								
Seawater (SW)				−0.41	0.01	−0.79	0.04	
Shallow sabkha groundwater (SGW)				−0.30	0.03	−0.59	0.08	
Lagoon water (SL)				−0.43	0.03	−0.82	0.05	

5.2. Magnesium isotope ratios

The δ^{26}Mg values of the analyzed (Sub-)Recent stoichiometric dolomite range between −1.09 and −0.38‰, with an average value of −0.79 ± 0.41‰ (2σ, n = 17; Table 1a, Figs. 5, 6). The mean δ^{26}Mg values of sabkha porewater range between −0.52‰ and −0.23‰, with an average of −0.45 ± 0.18‰ (2σ, n = 9). Tidal flat mud cores rSD3 and rSD1b show a distinct variation of porewater and dolomite δ^{26}Mg data with sediment depth (Fig. 6A, B). In core rSD1b, the $\delta^{26}Mg_{porewater}$ is nearly constant throughout the sediment core (−0.44 ± 0.06‰ 2σ), whereas $\delta^{26}Mg_{dol}$ shift to heavier values with increasing sediment depth (Fig. 6B). In contrast, in core rSD3 the dolomite is gradually enriched in light Mg isotope with increasing depth. The Mg isotope composition of the porewater shows the opposite trend for depths greater 30 cm (Fig. 6A).

The separate sampled waters are characterized by δ^{26}Mg values of −0.79‰ (±0.04 2σ, seawater), −0.59‰ (±0.08 2σ, shallow sabkha groundwater) and −0.82‰ (±0.05 2σ, lagoon water). Magnesium isotope values of water samples and calcite (−1.40‰ ± 0.04 2σ, n = 1), gypsum (−1.02‰ ± 0.08 2σ,n = 2) and microbial mat (−0.78‰ ± 0.19 2σ,n = 2) are given in Table 1a and shown in a three isotope plot in Fig. 5. The bulk sediment is characterized by a δ^{26}Mg value of −1.04‰ ± 0.28 (2σ, n = 2).

5.3. Elemental analysis

Table 1b summarizes major and trace elemental abundances of all water samples including seawater, lagoonal water and evaporated shallow sabkha groundwater and porewater. The lagoon water has a similar elemental distribution as observed for the seawater. The shallow groundwater and porewater are up to five-fold and ten-fold, respectively, enriched in Mg relative to the Mg content of the local seawater; ($Mg_{groundwater}$ = 7600 ppm: $Mg_{seawater}$ = 1500 ppm; $Mg/Ca_{??water}$ = 18.8: $Mg/Ca_{seawater}$ = 5). The Mg/Ca molar ratio of the porewater decreases with sediment depth from 75 (20 cm depth) to 27 (50 cm depth) within tidal flat mat core rSD3 and increases from 22 (20 cm depth) to 5 (37 cm depth) within tidal flat mat core rSD1b (Fig. 5B, D).

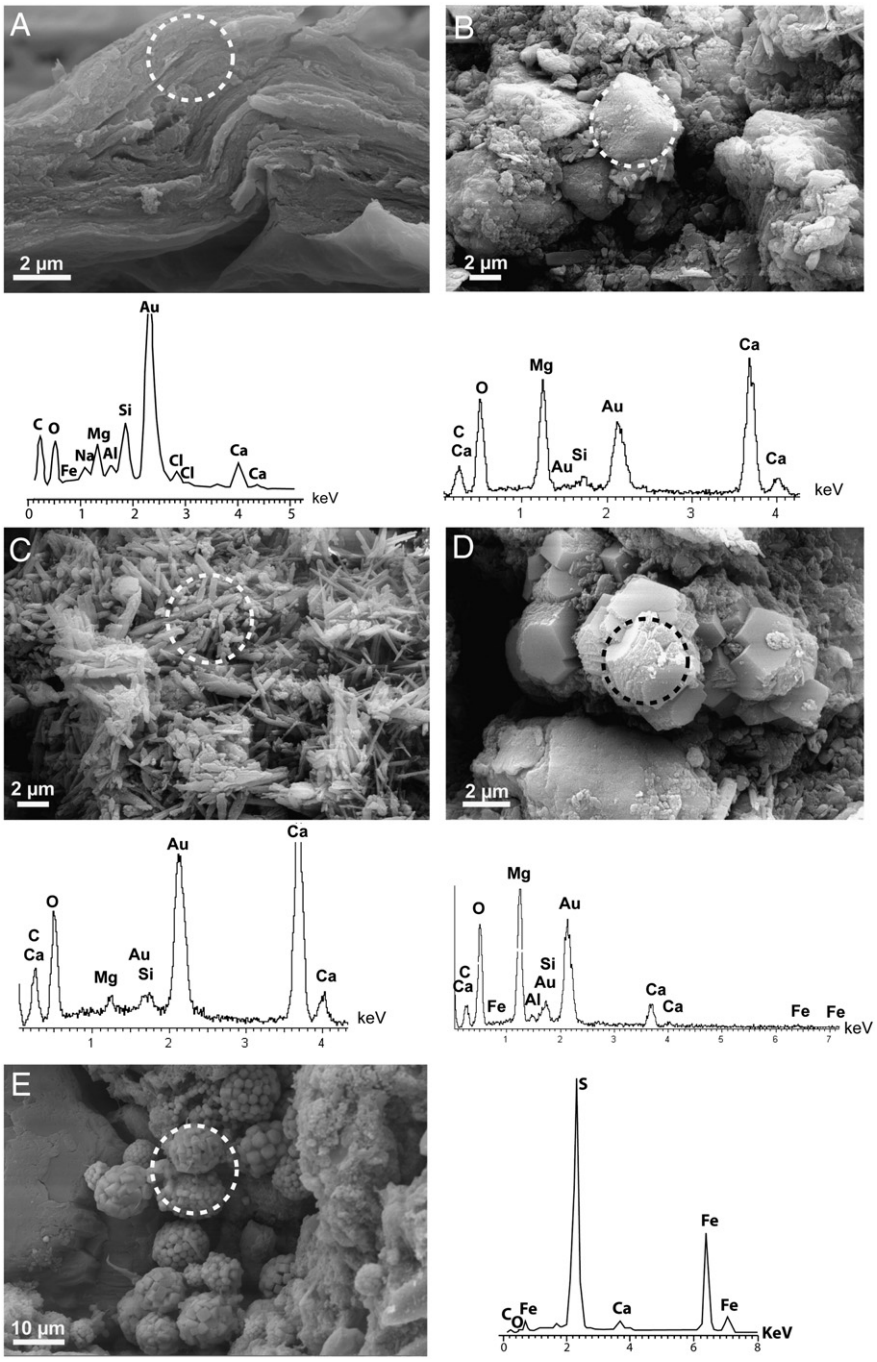

Fig. 3. Scanning electron photomicrograph showing mineral assemblages within the tidal flat core (rSD1b). A) Microbial mat layer, where EDX analyses indicate a mixture of silicates (most likely clay minerals) and organic material. In addition, the following minerals were detected with EDX: B) dolomite, C) aragonite needles, D) magnesite. The Au peak corresponds to the coating applied during preparation.

6. Interpretation and discussion

6.1. Magnesium isotope ratios of Mg bearing minerals and porewaters

In the shallow core material analyzed in this study dolomite is present as spherical agglomerates of small rhombohedral dolomite crystals as previously described by McKenzie and Vasconcelos (2009). The analyzed dolomites are well ordered (0.95), which is not exceptional when compared to low-temperature dolomites from previous field or laboratory studies (Vasconcelos and McKenzie, 1997; Roberts et al., 2004). Nevertheless, our data set is biased towards the most ordered end member of all Abu Dhabi sabkha dolomites as the protocol applied here does not discriminates between Mg-rich calcites and Ca-rich proto-dolomites that were dissolved prior to further analysis.

A detailed δ^{26}Mg data set including sabkha (i) mineral phases (dolomite, calcite and gypsum), (ii) microbial mat facies, and (iii) waters (local modern seawater, lagoonal water, sabkha shallow ground water and sabkha porewater) is compiled in Tables 1a and 1b.

The bulk sediment samples were taken from microbial mat layers and can be clearly distinguished in terms of their Mg isotopic composition from the chemically separated microbial mat- and dolomite samples (Fig. 5). The Mg isotopic composition of the bulk sediment sample

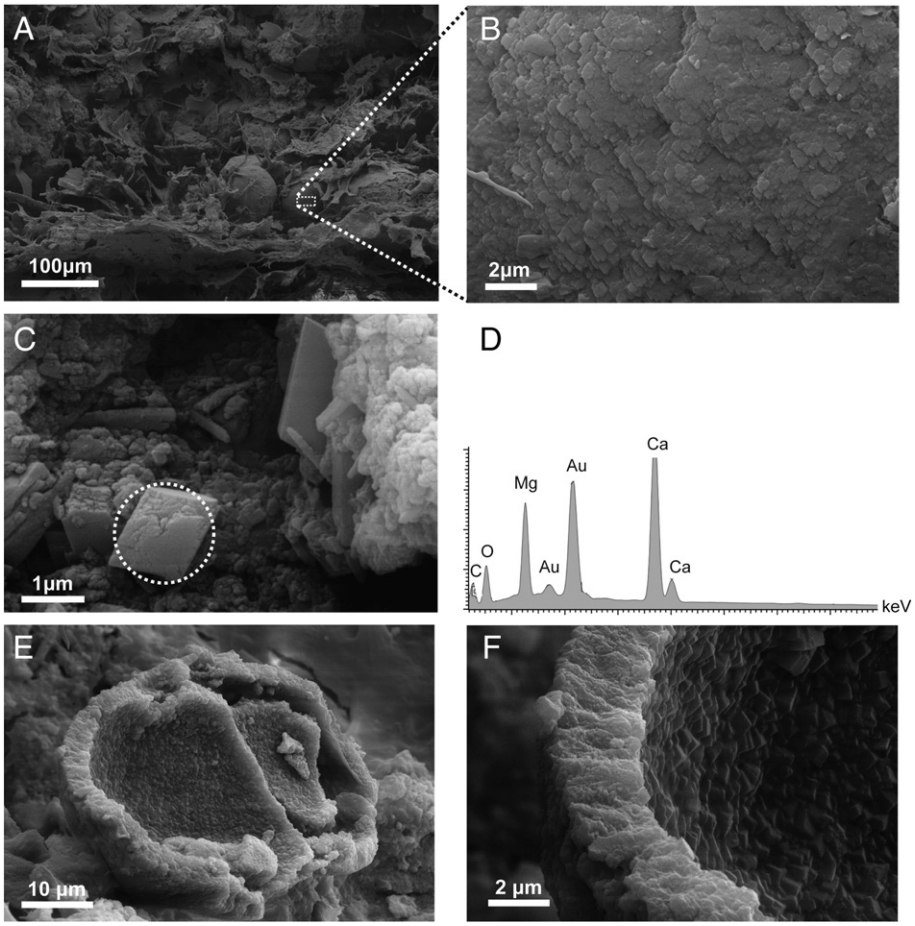

Fig. 4. A) SEM images of dolomite spheroids detected within buried microbial mat. B) Higher magnification of a dolomite spheroid indicates small-sized dolomite rhomboids. C) Single dolomite rhomboeder with D) EDX spectrum indicating a Ca–Mg carbonate composition. E) Dolomite encrusted mineral. F) Higher magnification of marked area in E).

($\delta^{26}Mg = -1.02‰$) reflect an admixture of the different Mg-bearing minerals (including calcite, Mg-calcite, dolomite, Mg bearing silicates, gypsum) and the organic Mg bearing microbial mat (e.g., chlorophyll; Black et al., 2006). This value confirms previous work by Azmy et al. (2013), who also analyzed bulk sediment samples from the Abu Dhabi sabkha environment ($\delta^{26}Mg_{mean}$ values of −1.03‰; n = 3). Particularly, the isotope composition of Mg incorporated in gypsum representing up to 14 wt.% of the sabkha sediment ($\delta^{26}Mg = -0.99‰$; Mg content = 1500 ppm), is similar to the bulk sediment $\delta^{26}Mg$ values. The separated sabkha dolomite $\delta^{26}Mg$ values range between −1.09‰ and −0.38‰ (mean = $-0.79 \pm 0.41‰$ 2σ, n = 17) and are therefore slightly depleted in ^{24}Mg compared to a diverse set of unspecified Precambrian dolomites reported in Pokrovsky et al. (2011) and an overview study on different fossil dolomite types Geske et al. (accepted for publication).

The calcite $\delta^{26}Mg$ mean value of −1.40‰ (Fig. 5) is within the range of previously published $\delta^{26}Mg$ values of limestones ranging between −4.59‰ and −1.0‰ (Tipper et al., 2006; Bolou-Bi et al., 2007; Brenot et al., 2008). The microbial mat itself has an Mg isotopic composition ($-0.78 \pm 0.19‰$ 2σ, n = 2) that is similar to that of marine phytoplankton samples of Ra and Kitagawa (2007) (chlorophyll α, β, χ) with $\delta^{26}Mg$ values ranging between −0.56 and +0.09‰ (Fig. 5). The chlorophyll in the microbial mat yields Mg isotopic ratios that are similar to that of the seawater samples ($\Delta^{26}Mg_{seawater-chlorophyll}$ = +0.3 to +0.7; Ra and Kitagawa, 2007). This implies that Mg in proto-dolomites and subsequently in dolomites might not only be derived from seawater but also from decaying organic (microbial) matter released to the surrounding porewater given that microbes are instrumental in the initial precipitation of proto-dolomites (Vasconcelos and McKenzie, 2008). Due to the <1‰ fractionation between seawater and organic microbial matter, however, this issue was not further investigated here.

The sabkha porewater is enriched in heavy Mg isotopes compared to seawater. Several mechanisms offer themselves: assuming closed system conditions, a solid containing the light isotopes of Mg is precipitated from a solution; the remaining solution is increasingly enriched in the heavy isotope (Rayleigh-type fractionation). Previous work indicates that ^{24}Mg strongly partitions into carbonate minerals, whereas Mg-bearing silicate minerals are characterized by partitioning of ^{26}Mg relative to the aqueous Mg (Tipper et al., 2006; Immenhauser et al., 2010; Bourdon et al., 2010; Li et al., 2012; Wimpenny et al., 2014a, 2014b). The magnesium isotopic composition of Mg bearing clay minerals is controlled by the relative proportion of structurally bounded Mg in the crystal lattice and the exchangeable intercalated or adsorbed Mg (Wimpenny et al., 2014a, 2014b). The latter can be easily leached and may act as Mg source during earliest diagenetic processes in the sabkha environment. Wimpenny et al. (2014a, 2014b) found, that exchangeable Mg of clay minerals is isotopically lighter (>1.5‰) than the $\delta^{26}Mg$ of the structural bound Mg. The acetic acid leachates (exchangeable Mg) of these clay minerals were found to range between −2.0 and −1.2‰ ($\delta^{26}Mg$). These values are comparable with typical diagenetically altered dolomite $\delta^{26}Mg$ values as reported in previous studies ($\delta^{26}Mg_{mean}$ of $-1.76 \pm 0.77‰$; n = 124; see references in Geske et al., accepted for publication). The $\delta^{26}Mg$ values of the clay residue (structural bound Mg) ranges between −0.2 and +0.6‰ (Wimpenny et al., 2014a, 2014b) and are consistent with results of clay residue analyzed in this study ($\delta^{26}Mg_{clay\ residue} = -0.2$, see Table A4) reflecting the mean magnesium isotopic composition of the upper continental crust ($\delta^{26}Mg_{UCC} = -0.22 \pm 0.10‰$; Li et al., 2010). However,

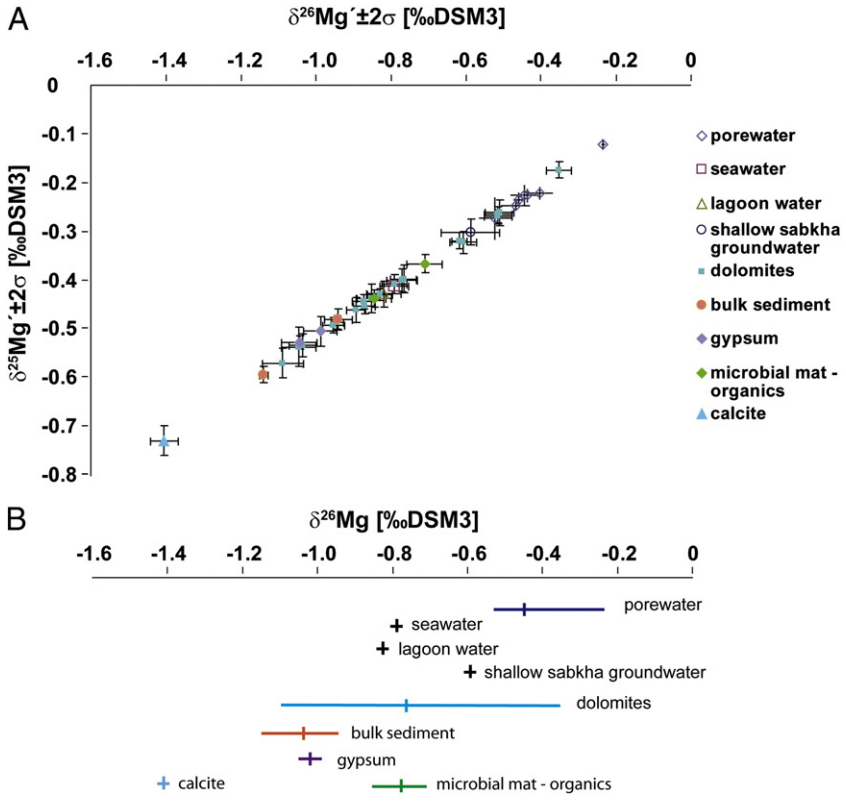

Fig. 5. A) Magnesium three isotope plot of all data investigated in this study including mineral, water and fluid samples. B) $\delta^{26}Mg_{mean}$ values of samples displayed in A).

based on the abundance of Mg in the saline pore water (12,000 to 16,000 ppm; Fig. 6a), estimates of the volume of aeolian clay minerals (5–14 wt.%) in the cores sampled and a simple mass balance, we conclude that sheet silicate-related exchangeable intercalated or adsorbed Mg was not a dominant factor affecting porewater of dolomite $\delta^{26}Mg$.

Nevertheless, sabkha shallow ground water sample $\delta^{26}Mg$ values (−0.59‰; Fig. 5) are coherent to $\delta^{26}Mg$ values of soil porewater ranging between −0.99‰ and −0.43‰ as documented in Tipper et al. (2010 and references therein), whereby in the case study of Tipper et al. (2010), the Mg was derived from weathered Mg bearing clay minerals in the basement. In the sabkha sediment, upward-leakage of deep groundwater from the underlying Cenozoic formations may or may not have transported Mg^{2+} ions from weathered basement silicates into the shallow groundwater (<1 m beneath sediment surface; Wood et al., 2002; Sanford and Wood, 2001). This process is not documented as such, but cannot be excluded a priori and might induce depth-gradients in the $\delta^{26}Mg$ isotope signature of sabkha porewater chemistry.

6.2. Impact of hydrodynamic level and sediment reworking

Depending on the site studied, sabkha depositional environments may remain largely undisturbed after deposition or undergo deposition, erosion and re-deposition. The agents of erosion are differential hydrodynamical levels including tidal currents or storm-related waves and currents events (Immenhauser, 2009). It is thus not surprising that tidal flat mud cores rSD1b and rSD3, spatially separated by a distance of less than 300 m, show a different, partly reverse lithostratigraphic succession (Figs. 1 and 2). Core rSD3 is characterized by a well laminated microbial mat and an undisturbed, protected intertidal sabkha succession including anhydrite/gypsum/halite layers overlying the microbial mat (Fig. 2B). Conversely, at Site 1b, the microbial mat facies is hydrodynamically reworked and the overlying stratigraphic levels including gypsum/anhydrite/halite intervals as observed at Site 3, which are lacking (Alsharhan and Kendall, 2003; Lokier and Steuber, 2008; Fig. 2A). Site 1b is situated landward in the upper intra-tidal zone and slightly older sediments were cored relative to Site 3, that is situated further seaward (Fig. 1). This general pattern is confirmed by C^{14} ages as documented in (Lokier and Steuber, 2008) revealing an age difference of about 160 yr.

With reference to magnesium isotope values obtained, sediment cores rSD1b and 3 are characterized by a completely different, partly reverse $\delta^{26}Mg$ pattern in terms of their porewater and dolomite relative to sediment depth (Fig. 6A, B). At Site 1b, the magnesium concentrations of the porewater in upper sediment layers increase (up to 10 cm sediment depth) and then decrease with depth, whereas the $\delta^{26}Mg_{porewater}$ values remain invariant (Fig. 6B). The $\delta^{26}Mg_{dolomite}$ values in the upper portion of the microbial mat facies trend to lighter values relative to the porewater and become enriched in heavy Mg isotopes with increasing sediment depth. In Site 3 the Mg isotope ratios of the dolomite trend to lighter values with increasing sediment depth, in contrast the porewater trend to heavier values downcore (Fig. 6A). In addition, the Mg content decreases with increasing depth.

Dolomites within cores in Site 1b and Site 3 are characterized by mean $\delta^{26}Mg$ values of −0.91‰ and −0.65‰, respectively, and are therefore depleted in ^{26} Mg relative to the porewater ($_{mean}$ = −0.44‰) and shallow sabkha groundwater ($\delta^{26}Mg$ water = −0.59‰). Site 3 dolomites are slightly enriched relative to modern Gulf seawater (seawater = −0.79‰), while the storm-reworked Site 1b is moderately depleted (Table 1a; Fig. 6). The diverging Mg isotope and concentration patterns of the porewater and dolomite observed at Site 3 are, at first glance, similar to reported in Higgins and Schrag (2010). Following Higgins and Schrag (2010), magnesium concentrations and magnesium isotopic compositions of porewaters reflect net precipitation of Mg-minerals (dolomite/Mg-clays) or local net sources.

Nevertheless, importance differences between the Higgins and Schrag (2010) data and those documented here are obvious: (i) Higgins and

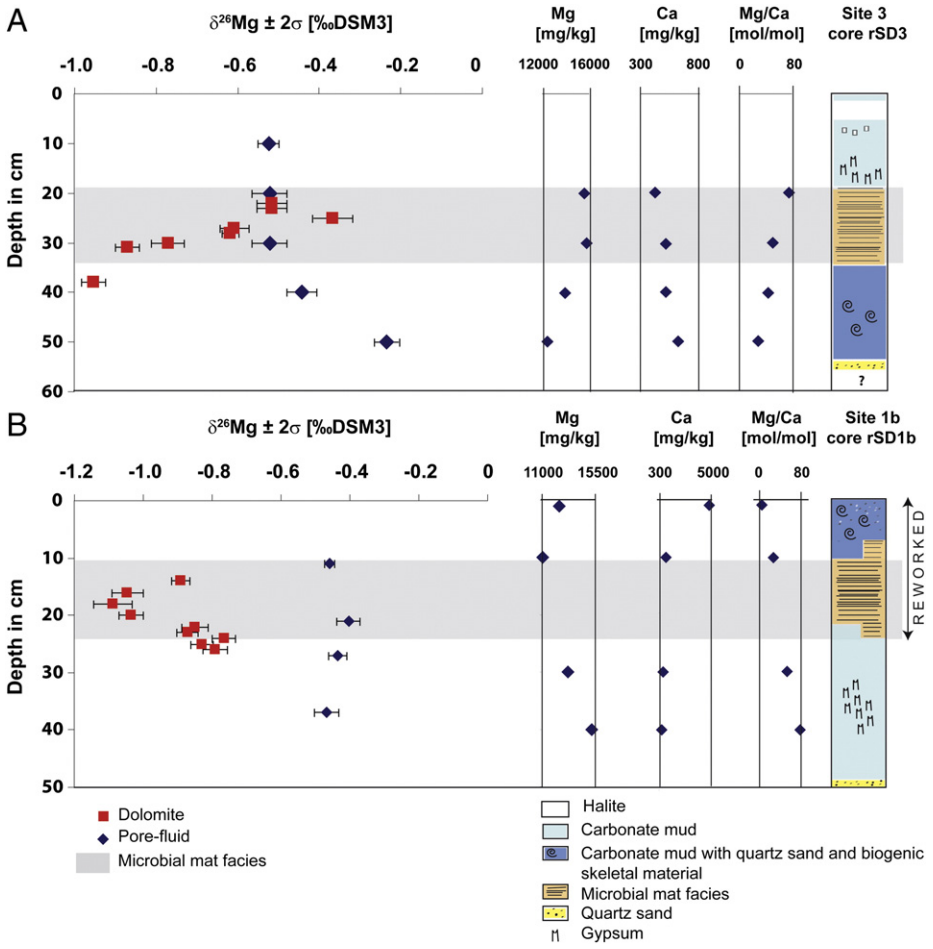

Fig. 6. A) Magnesium isotopic composition of dolomite (red squares) and (coeval?) porewater (blue rhombs) correlated with magnesium-, calcium concentrations, Mg/Ca molar ratios of the porewater relative to sediment depth in centimeter of logging Sites 3 (A) and 1b (B). The facies types of the sediment core are displayed on the right, where microbial mat layer are highlighted in gray rectangle. B) Same as A) for sampling Site 1b.

Schrag (2010) do not show data with a depth resolution of centimeters but data from cores with a length of between 250 and 750 m; (ii) the analyses in Higgins and Schrag (2010) are based on centrifuged bulk samples as opposed to the component-specific samples shown here; (iii) the clastic fraction of the samples in the cores studied by Higgins and Schrag (2010) is high (>60 wt.%) while it is low (<5 wt.%) in the case of the sabkha shallow cores; (iv) the dolomites described in Higgins and Schrag (2010) may include both, such related to anaerobic methane oxidation (AMO) and methanogenic dolomites while the later are not reported from the sabkha environment studied here (Bontognali et al., 2010); (v) the parent fluids in the cores described by Higgins and Schrag (2010) are shallow marine burial in origin while those studied here are evaporated marine sabkha fluids. This implies that data from these case studies are most likely not comparable.

Table 1b
Major and trace element contents of pore fluids and water samples.

Material	Facies	Sediment depth [cm]	Ca [mg/kg]	Mg [mg/kg]	Sr [mg/kg]	Fe [mg/kg]	Mg/Ca [mol/mol]
Tidal flat mud core rSD1b							
Porewater	Carbonate mud	1	4867	12,480	90	12	4.2
Porewater	Microbial mat	10	718	11,090	22	1	25.5
Porewater	Carbonate mud	30	420	13,210	14	2	51.8
Porewater	Carbonate mud	40	329	15,200	28	3	76.2
Tidal flat mud core rSD3							
Porewater	Microbial mat	20	353	16,000	13	1	74.7
Porewater	Microbial mat	30	537	16,210	16	4	49.8
Porewater	Carbonate mud	40	537	14,140	18	1	43.4
Porewater	Carbonate mud	50	750	12,470	25	1	27.4
Water samples							
Seawater (SW)			479	1498	10	0	5.2
Shallow sabkha groundwater (SGW)			664	7594	17	1	18.9
Lagoon water (SL)			571	1824	12	0	5.3

In the case of Site 3 (Fig. 6a), $\delta^{26}Mg_{dol}$ values shift to lighter values, with increasing core depth, while the $\delta^{26}Mg_{porewater}$ ratios shift to heavier values. Assuming closed system behavior, this may be linked to a preferential incorporation of light Mg isotopes (^{24}Mg) in the dolomite phase (but not necessarily with reference to other Mg-bearing phases), resulting in an enrichment of heavy isotopes (^{26}Mg) in the porewaters. Therefore, the precipitation of carbonate phases including dolomite actually has fractionated the remaining Mg pool of the porewater. The dolomite sample within the carbonate mud beneath the microbial mat (Fig. 6A) represents the lightest Mg isotope composition as calcite crystals in these layers may have act as Mg source during precipitation–dissolution reactions. Evidence for bacterial sulfate reduction processes with increasing sediment depth is euhedral pyrite (Fig. 3E), that is present within the carbonate mud below the microbial mat as a result of decomposition of organic matter (microbial mat; Berner et al., 1985).

At Site 1b, $\delta^{26}Mg_{dol}$ shifts to heavier values while the porewater $\delta^{26}Mg$ ratios remain near-constant with increasing core depth (Fig. 6B). Enrichment of ^{26} Mg dolomite phases with increasing sediment depth may result from the preferred incorporation of^{24} Mg in gypsum and/or calcite/Mg-calcite minerals in the underlying sediment. Sediment reworking is reflected by the scatter in $\delta^{26}Mg$ dolomite values within the sediment column of Site 1b (Fig. 6B). An important, but unresolved question is if dolomite precipitation and/or earliest diagenetic dolomite stabilization pre- or post-dates storm reworking (or both)? Sediment reworking in the upper portions of the core rSD1b (Site 1b) is evident from the lack of evaporates that is replaced by a proximal storm lag deposit, rich in biogenic skeletal material, above the microbial mat facies (Fig. 2A). The reasons for the loss of evaporative minerals may include storm flood recharge or high spring tides. Under these conditions, seawater, undersaturated with respect to gypsum/anhydrite/halite, is rapidly circulated through the sediments and dissolves portions or all of the evaporative minerals (Hsü and Siegenthaler, 1969). Circumstantial geochemical evidence comes from comparably depleted fluid Mg/Ca ratios in the upper part of the core that are similar to seawater Mg/Ca ratios ($Mg/Ca_{seawater}$ of 5). Flood recharge may also cause a downward seeping of storm surge water, features that may be reflected in the increasing Mg/Ca molar ratios of the porewater brine with increasing sediment depth (Fig. 6B). Summing up, it is concluded that seawater diluted the sabkha porewater near-surface portions of the sediment while downcore the porewater dominated the system (mixing $ratio_{seawater-porewater}$). Nevertheless, storm reworking might have taken place years ago and downward seeping seawater might was possibly affected by some degree of subsequent evaporation. In essence, the comparison of the two cores documents the complexity of natural systems and the limitations of field based studies.

6.3. Apparent magnesium isotope fractionation between sabkha porewater and stoichiometric dolomite

Owing to the bias of our dolomite samples towards the most ordered phase (>0.9), we lack a series of data linking differential degrees of order with corresponding $\delta^{26}Mg_{dol}$. Consequently, the following discussion refers to the ordered end-member of the Abu Dhabi sabkha dolomite population. The main Mg source in the sabkha environment is evaporated seawater. Major factors that affect the apparent fractionation factor $\Delta^{26}Mg_{dol\text{-}Mg(porewater)}$ of sabkha dolomites may include (i) non-equilibrium processes such as microbial activity (Shirokova et al., 2011), (ii) dehydratization of aqueous Mg^{2+} during incorporation in the non-stoichiometric dolomite or highest Mg calcite (Immenhauser et al., 2010; Mavromatis et al., 2013; Li et al., 2014), or (iii) geochemical resetting during the earliest diagenetic transformation of non-stoichiometric to stoichiometric dolomite. The latter assumption bases on the concept that non-stoichiometric dolomites release Ca while they take up Mg from their ambient porewater. This may lead to the observed strong partitioning of light Mg isotopes in carbonates but suggest a rather conservative behavior once dolomites are well-ordered. This pattern is possibly observed in Fig. 5 documenting a depletion of mean $\delta^{26}Mg_{dol}$ (−0.79‰) relative to mean $\delta^{26}Mg_{porewater}$ (−0.23‰; Table 1a).

Carder et al. (2005) showed that microbially-induced dolomite in hypersaline lagoons in South America is isotopically lighter by −0.49 to −3.07‰ relative to the parent water but this probably refers to non-stoichiometric dolomites. In comparison, the $\Delta^{26}Mg_{dol\text{-}Mg(porewater)}$ shown here ranges between −0.3‰ and +0.7‰ (Site 1b) and −0.5 and +0.1‰ (Site 3) depending on the stratigraphic level sampled (Table 1a, Fig. 6) thus moderate fractionation is observed. As such, the variable apparent $\Delta_{26}Mg_{dol\text{-}Mg(porewater)}$ as observed here is expected in a complex, multi-parameter natural system such as the one studied here. We emphasize that the data shown here cannot be compared with measured fractionation factors obtained from strictly controlled, abiogenic precipitation experiments in laboratories.

Moreover, the age of the dolomites extracted from these cores may range from some years to maximum of about 1500 years as based on radiocarbon age data (Lokier and Steuber, 2008). Hence, even in these sub-recent settings, we cannot exclude that the present-day sabkha porewater values are representative for that of the last millennium. This may explain the intriguing positive apparent fractionation factors potentially reflecting transient periods of more positive porewater values. Hence, while the data shown in Carder et al. (2005) differ from those shown here, both studies clearly document that one must not expect constant $\Delta^{26}Mg_{dol\text{-}Mg(porewater)}$ in natural settings.

Nevertheless, the apparent $\Delta^{26}Mg_{dol\text{-}Mg(porewater)}$ values found here are comparably small relative to previously documented values reported by Higgins and Schrag (2010, 2012) or Carder et al. (2005). With reference to South American saline lagoon dolomites reported in Carder et al. (2005), differential microbial metabolism (Abed et al., 2008; Bolou-Bi et al., 2010) might be of significance and the cited references do not clearly specify the degree of order of dolomites studied. Specifically, these authors propose a vital disequilibrium fractionation effect due to bioactivity within the sediment that covers a wide $\delta^{26}Mg$ range of $+0.09 \pm 0.22$ to -3.55 ± 0.29‰ depending on the organism investigated.

Alternative reasons for the differential fractionation factors as documented in Higgins and Schrag (2010) may include early diagenetic porewater alteration of Upper Miocene to Upper Pleistocene dolomites and/or different environmental physicochemical parameters (e.g., temperature, precipitation rates, aqueous Mg concentration and pH). Supporting evidence for this perhaps comes from the work of Vasconcelos and McKenzie (1997). These authors found, that at sediment depths from 10 to 15 cm, microbially induced dolomite changes its mole% Mg (39 to 48) composition indicating a very early diagenetic trend towards more stoichiometric dolomite phases mediated by microbial activity. Direct evidence for earliest porewater diagenesis in Recent sabkha dolomites might include the change in dolomite texture with increasing sediment depth as observed in the cores here (Fig. 4). Dolomite spheroids, detected in microbial mats (Fig. 3), subsequently disintegrate to smaller rhombohedral crystals with increasing sediment depth. These considerations are of importance as our data set is biased towards the most ordered end-member spectrum of (Sub-)Recent dolomites in the Abu Dhabi sabkha depositional environment.

Summing up, the data shown here might indicate that the significant $\Delta^{26}Mg_{dol\text{-}Mg(porewater)}$ values as reported in Higgins and Schrag (2010) might represent a more advanced stage of stabilization of Neogene dolomites including early diagenetic resetting and exchange between aqueous Mg in the porewater and Mg contained in the dolomite crystal lattice. In this sense, the (Sub-)Recent sabkha dolomite data presented here may document an earlier stage of dolomite geochemistry affected by re-equilibration compared to the older more stabilized ones shown in Higgins and Schrag (2010). Evidence for the possibly increasing $\Delta^{26}Mg_{dol\text{-}Mg(porewater)}$ with time comes from the diagenetically altered Pleistocene sabkha dolomites, sampled in the northern Gulf region

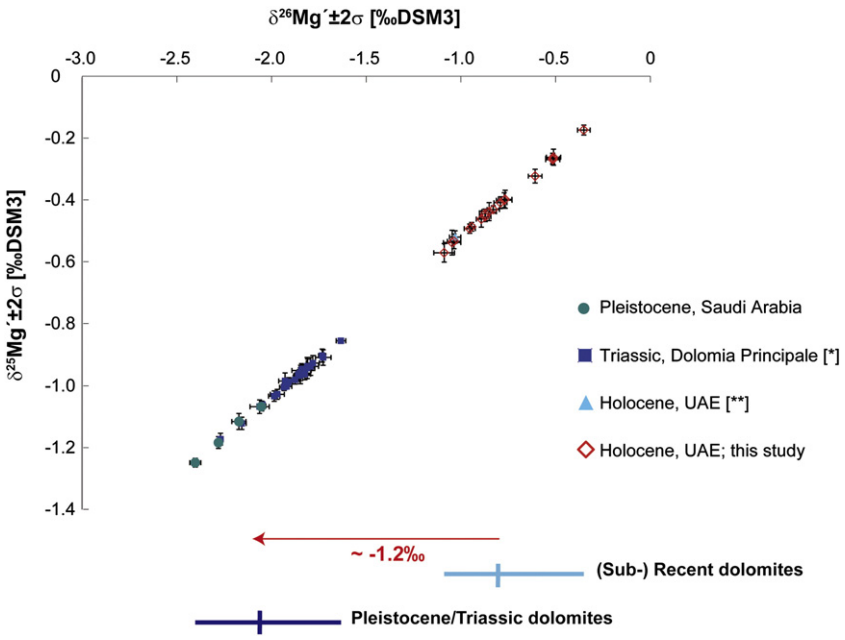

Fig. 7. Comparison between the magnesium isotopic compositions of Recent sabkha dolomites and fossil Pleistocene as well as Triassic sabkha dolomites. The difference in mean Mg isotope compositions between Recent and fossil sabkha dolomites is −1.2‰ with Pleistocene and Triassic sabkha dolomites being remarkable similar in their mean δ^{26}Mg isotope ratios. These data sets involve published data from [*] Geske et al. (2012) and [**] Azmy et al. (2013).

(Saudi Arabia; Chafetz and Rush, 1994), those are significantly more depleted in ^{26} Mg relative to the (Sub-)Recent sabkha dolomites.

6.4. Comparing δ^{26}Mg ratios of recent and ancient sabkha dolomites

Fig. 7 and Table 2 summarize the δ^{26}Mg values of (Sub-)Recent, Pleistocene and Triassic sabkha dolomites. Magnesium-isotope values of Triassic Dolomia Principale sabkha dolomites as reported in Geske et al. (2012; $\delta^{26}Mg_{D2}$ mean: -1.89 ± 0.33‰, n = 28) and sabkha dolomites of Pleistocene age from Al Jubayl, Saudi Arabia are documented in Table 2 (δ^{26}Mg mean: -2.22 ± 0.30‰, n = 4) and overlap in their magnesium isotopic composition. Conversely, (Sub-)Recent sabkha dolomites as reported in this study are enriched in ^{26} Mg by up to 1.2 or 1.4‰, respectively, compared to Pleistocene and Triassic sabkha dolomites (Fig. 7). Particularly the comparison of sabkha dolomites of different ages in the Gulf Region is relevant for this discussion. Given the long $Mg_{seawater}$ residence times of τ ~13 Myr (Broecker and Peng, 1982), the observed ($\Delta^{26}Mg_{dol(Recent)-dol(Pleistocene)}$ = 1.4‰) cannot be explained by fluctuations in seawater δ^{26}Mg ratios over the last 2.6 Myr. Moreover, the coastal morphology, hydrology, sediment composition, level of aridity is similar when comparing the Recent and the Pleistocene sabkha in the Gulf (Purser and Evans, 1973; Williams and Walkden, 2002; Atkinson et al., 2013). Therefore, the degree of post-precipitation magnesium isotope re-equilibration must be considered.

Summing up, the differential geochemistry between Sub-recent and fossil sabkha dolomites is perhaps best interpreted in the sense of (semi)open-system, earliest diagenetic exchange between dolomite crystals and porewater affecting the δ^{26}Mg signature of increasingly stoichiometric dolomites. With reference to the Triassic sabkha dolomites documented in Geske et al. (2012), the unknown $\delta^{26}Mg_{seawater}$ ads further complexity. While earliest, non-stoichiometric (microbial, degree of order = 02.–0.7; McKenzie, 1981) and earliest stoichiometric dolomites (degree of order >0.9) reported here, are characterized by subdued $\Delta^{26}Mg_{dol\text{-}Mg(porewater)}$, the increasing loss of Ca^{2+} and uptake of Mg^{2+} from, or in the case of stoichiometric dolomites, the exchange with the ambient porewater leads to an increasing depletion of $\delta^{26}Mg_{dol}$ relative to $\delta^{26}Mg_{porewater}$.

7. Conclusions

This study reports on the apparent fractionation of Mg isotopes between stoichiometric (Sub-)Recent sabkha dolomites and their ambient evaporated porewater. Magnesium isotope values of recent well-ordered dolomite samples range between −1.09 and −0.38‰, with an average of −0.79‰ ±0.41 (2σ, n = 17). The mean δ^{26}Mg values of sabkha porewater samples range between −0.52‰ and −0.23‰, with an average of -0.45 ± 0.18‰ (2σ, n = 9). Thus, ambient sabkha porewaters are enriched in +0.43‰ relative to modern seawater δ^{26}Mg. Individual apparent $\Delta^{26}Mg_{dol\text{-}Mg(porewater)}$ values range from

Table 2
Magnesium isotopic composition of Pleistocene, Triassic and Holocene sabkha dolomite samples.

Sample	Age	Sampling site	δ^{26}Mg [‰ DSM3]	±2σ	δ^{25}Mg [‰ DSM3]	±2σ
This study n = 17	Holocene	Abu Dhabi, UAE	−0.79	0.41		
Ds[a] n = 3	Holocene	Abu Dhabi, UAE	−1.03	0.03		
B31a	Pleistocene	Al Jubayl, Saudi Arabia	−2.17	0.04	−1.12	0.03
B31b	Pleistocene	Al Jubayl, Saudi Arabia	−2.28	0.02	−1.18	0.02
B31c	Pleistocene	Al Jubayl, Saudi Arabia	−2.40	0.03	−1.25	0.01
B30	Pleistocene	Al Jubayl, Saudi Arabia	−2.05	0.02	−1.07	0.01
Dolomia Principale[b] n = 28	Upper Triassic	Alpine Realm (Austria, Italy)	−1.89	0.33		

[a] Azmy et al. (2013).
[b] Geske et al. (2012).

−0.7 to +0.1‰, which is significantly smaller than those reported in previous studies. The variability range in the isotope fraction observed is, *per se*, comparable with data from Recent saline lagoons in South America, while absolute numbers differ significantly. Mechanisms involved are complex but may include net precipitation of Mg-minerals (dolomite/Mg-clays) with preferential partitioning of Mg into carbonate phases or local net sources within the tidal flat mud cores. Variations in magnesium isotopic compositions of dolomites go along with changes in Mg/Ca molar ratios of the porewater. With increasing sediment depth the aqueous Mg/Ca molar ratio decreases in an undisturbed tidal flat mat core (rSD3, Site 3) while another core has been affected by storm reworking core (rSD1b, Site 3). Pleistocene sabkha dolomites from Al Jubayl, Saudi Arabia are enriched in ^{24} Mg relative to (Sub-)Recent ones by up to ~1.2‰. The data shown here document the complexity and limitations of natural laboratories. Given the differences between seawater and evaporated marine porewater δ^{26}Mg and the remarkably complex kinetic and dissolution/precipitation and source-sink reactions, ancient sabkha dolomites should not be viewed as direct archive of coeval $\delta^{26}Mg_{seawater}$.

Acknowledgments

Our thanks go to the staff of the non-traditional isotope laboratory of the Ruhr-University Bochum, particularly Dr. D. Buhl and B. Gehnen. Dr. V. Mavromatis is acknowledged for his rigorous comments on a previous version of this paper. We thank H.S. Chefetz for sending us Pleistocene sabkha samples from Al Jubayl, Saudi Arabia. Chemical Geology associate editor M.E. Böttcher and two anonymous reviewers are greatly acknowledged for detailed and insightful comments.

Appendix A. Supplementary data

Supplementary data to this article can be found online at http://dx.doi.org/10.1016/j.chemgeo.2014.11.020.

References

Abed, R.M.M., Kohls, K., Schoon, R., Scherf, A.-K., Schacht, M., Palinska, K.A., Al-Hassani, H., Hamza, W., Rullkötter, J., Golubic, S., 2008. Lipid biomarkers, pigments and cyanobacterial diversity of microbial mats across intertidal flats of the arid coast of the Arabian Gulf (Abu Dhabi, UAE). FEMS Microbiol. Ecol. 65, 449–462.

Alsharhan, A.S., Kendall, C.G.St.C., 2003. Holocene coastal carbonates and evaporites of the southern Arabian Gulf and their ancient analogues. Earth Sci. Rev. 61, 191–243.

Atkinson, O.A.C., Thomas, D.S.G., Parker, A.G., Goudie, A.S., 2013. Late Quaternary humidity and aridity dynamics in the northeast Rub' al-Khali. United Arab Emirates:Implications for early human dispersal and occupation of eastern Arabia. Quaternary International. 300, 292–301.

Azmy, K., Lavoie, D., Wang, Z., Brand, U., Al-Aasm, I., Jackson, S., Girard, I., 2013. Magnesium isotope and REE composition of Lower Ordovician carbonates from eastern Laurentia: implications for the origin of dolomites and limestones. Chem. Geol. 356, 64–75.

Babcock, R.S., Atwood, D.K., Perry, D., 1967. Separation of dolomite from fine grained recent sediments. Am. Mineral. 52, 1563–1567.

Baltzer, F., Kenig, F., Boichard, R., Plaziat, J.-C., Purser, B.H., 1994. Organic matter distribution, water circulation and dolomitization beneath the Abu Dhabi Sabkha (United Arab Emirates). In: Purser, B., Tucker, M., Zenger, D. (Eds.), Dolomites — A Volume in Honour of Dolomieu. Blackwell Scientific Publications, International Association of Sedimentologists, Special Publications, pp. 409–427.

Berner, R.A., De Leeuw, J.W., Spiro, B., Murchison, D.G., Eglinton, G., 1985. Sulphate reduction, organic matter decomposition and pyrite formation. Philos. Trans. R. Soc. 315, 25–38.

Black, J.R., Yin, Q.-Z., Casey, W.H., 2006. An experimental study of magnesium-isotope fractionation in chlorophyll-a photosynthesis. Geochim. Cosmochim. Acta 70, 4072–4079.

Bodine, M.W., Fernalld, T.H., 1973. EDTA dissolution of gypsum, anhydrite and Ca–Mg carbonates. J. Sediment. Petrol. 43, 1152–1156.

Bolou Bi, E.B., Vigier, N., Poszwa, A., Brenot, A., 2007. Compared magnesium isotope compositions of plants, rocks and waters. Geochim. Cosmochim. Acta 71.

Bolou-Bi, E.B., Poszwa, A., Leyval, C., Vigier, N., 2010. Experimental determination of magnesium isotope fractionation during higher plant growth. Geochim. Cosmochim. Acta 74, 2523–2537.

Bontognali, T.R.R., Vasconcelos, C., Warthmann, R.J., Bernasconi, S.M., Dupraz, C., Strohmenger, C.J., McKenzie, J.A., 2010. Dolomite formation within microbial mats in the coastal sabkha of Abu Dhabi (United Arab Emirates). Sedimentology 57, 824–844.

Bourdon, B., Tipper, E.T., Fitoussi, C., Stracke, A., 2010. Chondritic Mg isotope composition of the Earth. Geochim. Cosmochim. Acta 74, 5069–5083.

Brenot, A., Cloquet, C., Vigier, N., Carignan, J., France-Lanord, C., 2008. Magnesium isotope systematics of the lithologically varied Moselle river basin, France. Geochim. Cosmochim. Acta 72, 5070–5089.

Broecker, W.S., Peng, T.-H., 1982. Tracers in the Sea. Lamont-Doherty Geological observatory, Colombia university, Palisades, NY, p. 10964.

Butler, G.P., 1969. Modern evaporate deposition and geochemistry of coexisting brines, the sabkha, Trucial Coast, Arabian Gulf. J. Sediment. Petrol. 39, 70–89.

Carder, E.A., Galy, A., McKenzie, J.A., Vasconcelos, C., Elderfield, H.E., 2005. Magnesium isotopes in bacterial dolomites: a novel approach to the dolomite problem. Geochim. Cosmochim. Acta 69, A213.

Chafetz, H.S., Rush, P.F., 1994. Diagenetically altered sabkha-type Pleistocene dolomite from the Arabian Gulf. Sedimentology 41, 409–421.

Compton, J.S., 1988. Degree of supersaturation and precipitation of organogenic dolomite. Geology 16, 318–321.

Deng, S., Dong, H., Lv, G., Jiang, H., Yu, B., Bishop, M.E., 2010. Microbial dolomite precipitation using sulfate reducing and halophilic bacteria: results from Qinghai Lake, Tibetan Plateau, NW China. Chem. Geol. 278, 151–159.

Evans, G., Schmidt, V., Bush, P., Nelson, H., 1969. Stratigraphy and geologic history of the Sabkha, Abu Dhabi, Persian Gulf. Sedimentology 12, 145–159.

Füchtbauer, H., Goldschmidt, H., 1965. Beziehungen zwischen Calcium-Gehalt und Bildungsbedingungen der Dolomite. Geol. Rundsch. 55, 29–40 (Stuttgart).

Füchtbauer, H., Richter, D.K., 1988. Karbonatgesteine. In: Füchtbauer (Ed.), Sedimente und Sedimentgesteine, pp. 233–434 (Stuttgart).

Galy, A., Belshaw, N.S., Halicz, L., O'Nions, R.K., 2001. High-precision measurements of magnesium isotopes by multiple-collector inductively coupled plasma mass spectrometry. Int. J. Mass Spectrom. 89–98.

Galy, A., Yoffe, O., Janney, P.E., Williams, R.W., Cloquet, C., Alard, O., Halicz, L., Wadwha, M., Hutcheon, I.D., Ramon, E., Carignan, J., 2003. Magnesium isotopes heterogeneity of the isotopic standard SRM980 and new reference materials for magnesium-isotope-ratio measurements. J. Anal. At. Spectrom. 18, 1352–1356.

Geske, A., Zorlu, J., Richter, D.K., Buhl, D., Niedermayr, A., Immenhauser, A., 2012. Impact of diagenesis and low grademetamorphosis on isotope (δ^{26}Mg, δ^{13}C, δ^{18}O and ^{87}Sr/^{86}Sr) and elemental (Ca, Mg, Mn, Fe and Sr) signatures of Triassic sabkha dolomites. Chem. Geol. 332–333, 45–64.

Geske, A., Goldstein, R.H., Mavromatis, V., Richter, D.K., Kluge, T., John, C.M., Immenhauser, A., 2015. The magnesium isotope (δ^{26}Mg) signatures of dolomites. Geochim. Cosmochim. Acta 131–151.

Glover, E.D., 1961. Method of solution of calcareous materials using the complexing agent EDTA. J. Sediment. Petrol. 31, 622–626.

Hardie, L.A., 1987. Perspectives dolomitization: a critical view of some current views. J. Sediment. Petrol. 57, 166–183.

Hardy, R., Tucker, M., 1988. X-ray powder diffraction of sediments. In: Tucker, M.E. (Ed.), Techniques in Sedimentology. Blackwell Scientific Publications, Oxford, pp. 191–228.

Higgins, J.A., Schrag, D.P., 2010. Constraining magnesium cycling in marine sediments using magnesium isotopes. Geochim. Cosmochim. Acta 74, 5039–5053.

Higgins, J.A., Schrag, D.P., 2012. Records of Neogene seawater chemistry and diagenesis in deep-sea carbonate sediments and pore fluids. Earth Planet. Sci. Lett. 357–358, 386–396.

Hippler, D., Buhl, D., Witbaard, R., Richter, D.K., Immenhauser, A., 2009. Towards a better understanding of magnesium-isotope ratios from marine skeletal carbonates. Geochim. Cosmochim. Acta 73, 6134–6146.

Hsü, K.J., Siegenthaler, C., 1969. Preliminary experiments on hydrodynamic movement induced by evaporation and their bearing on the dolomite problem. Sedimentology 12, 11–25.

Illing, L., Wells, A.J., Taylor, J.C.M., 1965. Penecontemporary dolomite in the Persian Gulf. In: Pray, L.C., Murray, R.C. (Eds.), Dolomitiztion and Limestone Diagenesis: SEPM Special Publication, pp. 89–111.

Immenhauser, A., 2009. Estimating palaeo-water depth from the physical rock record. Earth Sci. Rev. 96, 107–139.

Immenhauser, A., Buhl, D., Richter, D., Niedermayr, A., Riechelmann, D., Dietzel, M., Schulte, U., 2010. Magnesium-isotope fractionation during low-Mg calcite precipitation in a limestone cave — field study and experiments. Geochim. Cosmochim. Acta 74, 4346–4364.

Kenward, P.A., Goldstein, R.H., González, L.A., Roberts, J.A., 2009. Precipitation of low-temperature dolomite from an anaerobic microbial consortium: the role of methanogenic Archaea. Geobiology 7, 556–565.

Kinsman, D.J.J., 1969. Modes of formation, sedimentary associations, and diagnostic features of shallow-water and supratidal evaporites. AAPG Bull. 53, 830–840.

Last, F.M., Last, W.M., Halden, N.M., 2012. Modern and late Holocene dolomite formation: Manito Lake, Saskatchewan, Canada. Sediment. Geol. 281, 222–237.

Li, W.-Y., Teng, F.-Z., Ke, S., Rudnick, R.L., Gao, S., Wu, F.-Y., Chappell, B.W., 2010. Heterogeneous magnesium isotopic composition of the upper continental crust. Geochim. Cosmochim. Acta 74, 6867–6884.

Li, W.-Y., Chakraborty, S., Beard, B.I., Romanek, C.S., Johnson, V.M., 2012. Magnesium isotope fractionation during precipitation of inorganic calcite under laboratory conditions. Earth Planet. Sci. Lett. 333–334, 304–316.

Li, W., Beard, B.L., Li, C., Johnson, C.M., 2014. Magnesium isotope fractionation between brucite [$Mg(OH)_2$] and Mg aqueous species: implications for silicate weathering and biogeochemical processes. Earth Planet. Sci. Lett. 394, 82–93.

Lokier, S.W., 2012. Development and evolution of subaerial halite crust morphologies in a coastal sabkha setting. J. Arid Environ. 79, 32–47.

Lokier, S., Steuber, T., 2008. Quantification of carbonate-ramp sedimentation and progradation rates for the Late Holocene Abu Dhabi shoreline. J. Sediment. Res. 78, 423–431.

Lokier, S., Steuber, T., 2009. Large-scale intertidal polygonal features of the Abu Dhabi coastline. Sedimentology 56, 609–621.
Mavromatis, V., Gautier, Q., Bosc, O., Schott, J., 2013. Kinetics of Mg partition and Mg stable isotope fractionation during its incorporation in calcite. Geochim. Cosmochim. Acta 114, 188–203.
Mazzullo, S.J., 2000. Oranogenic dolomitization in peritidal to deep-sea sediments. J. Sediment. Res. 70, 10–23.
McKenzie, J.A., 1981. Holocene dolomitization of calcium carbonate sediments from the coastal sabkhas of Abu Dhabi, U.A.E.: a stable isotope study. J. Geol. 89, 185–198.
McKenzie, J.A., Vasconcelos, C., 2009. Dolomite mountains and the origin of the dolomite rock of which they mainly consists, historical developments and new perspectives. Sedimentology 56, 205–219.
McKenzie, J.A., Hsü, K.J., Schneider, J.F., 1980. Movement of subsurface waters under the Sabkha, Abu Dhabi, UAE, and its relation to evaporative dolomite genesis. In: Zenger, D.H., Dunham, J.B., Ethington, R.L. (Eds.), Concepts and Models of Dolomitization, pp. 11–30.
Ostrom, M.E., 1961. Separation of clay minerals from carbonate rocks by using acid. J. Sediment. Petrol. 31, 123–125.
Patterson, R.J., Kinsman, D.J.J., 1977. Marine and continental sources in a Persian Gulf coastal sabkha. In: Frost, S.H., Weiss, M.P., Saunders, J.B. (Eds.), Reefs and Related Carbonates: Ecology and Sedimentology. Am Assoc Pet Geol Stud Geol, pp. 381–397.
Pokrovsky, B.G., Mavromatis, V., Pokrovsky, O.S., 2011. Co-variation of Mg and C isotopes in late Precambrian carbonates of the Siberian Platform: a new tool for tracing the change in weathering regime? Chem. Geol. 290, 67–74.
Purser, B.H., Evans, G., 1973. Regional sedimentation along the Trucial Coast, SE Persian Gulf. In: Purser, B.H. (Ed.), The Persian Gulf — Holocene Carbonate Sedimentation and Diagenesis in a Shallow Epicontinental Sea. Springer-Verlag, Berlin, pp. 211–231.
Purser, B.H., Tucker, M.E., Zenger, D.H., 1994. Problems, progress and future research concerning dolomites and dolomitization. In: Purser, B.H., Tucker, M.E., Zenger, D.H. (Eds.), Dolomites: A Volume in Honour of Dolomieu. Blackwell Scientific Publications, Oxford, pp. 3–28.
Ra, K., Kitagawa, H., 2007. Magnesium isotope analysis of different chlorophyll forms in marine phytoplankton using multi-collector ICP-MS. J. Anal. At. Spectrom. 22, 817–821.
Roberts, J., Bennett, P.C., González, L.A., Macpherson, G.L., Milliken, K.L., 2004. Microbial precipitation of dolomite in methanogenic groundwater. Geology 32, 277–280.
Roberts, J.A., Kenward, P.A., Fowle, D.A., Goldstein, R.H., González, L.A., Moore, D.S., 2013. Surface chemistry allows for abiotic precipitation of dolomite at low temperature. Proc. Natl. Acad. Sci. 110, 14540–14545.
Sánchez-Román, M., Vasconcelos, C., Schmid, T., Dittrich, M., McKenzie, J.A., Zenobi, R., Rivadeneyra, M.A., 2008. Aerobic microbial dolomite at the nanometer scale: implications for the geologic record. Geology 36, 879–882.
Sánchez-Román, M., McKenzie, J.A., De Luca Rebello Wagener, A., Rivadeneyra, M.A., Vasconcelos, C., 2009. Presence of sulfate does not inhibit low-temperature dolomite precipitation. Earth Planet. Sci. Lett. 285, 131–139.
Sánchez-Román, M., McKenzie, J.A. Luca, Rebello Wagener, A., Romanek, C.S., Sánchez-Navas, A., Vasconcelos, C., 2011. Experimentally determined biomediated Sr partition coefficient for dolomite: significance and implication for natural dolomite. Geochim. Cosmochim. Acta 75, 887–904.
Sanford, W.E., Wood, W.W., 2001. Hydrology of the coastal sabkhas of Abu Dhabi, United Arab Emirates. Hydrogeol. J. 9, 358–366.
Shirokova, L.S., Mavromatis, V., Bundeleva, I., Pokrovsky, O.S., Bénézeth, P., Pearce, C., Gérard, E., Balor, S., Oelkers, E.H., 2011. Can Mg isotopes be used to trace cyanobacteria-mediated magnesium carbonate precipitation in alkaline lakes? Biogeosci. Discuss. 8, 6473–6517.
Tipper, E.T., Bickle, M.J., Galy, A., West, A.J., Pomies, C., Chapman, H.J., 2006. The short term sensitivity of carbonates and silicate weathering fluxes: insight from seasonal variations in river chemistry. Geochim. Cosmochim. Acta 70, 2737–2754.
Tipper, E.T., Gaillardet, J., Louvat, P., Capmas, F., White, A.F., 2010. Mg isotope constraints on soil pore-fluid chemistry: evidence from Santa Cruz, California. Geochim. Cosmochim. Acta 74, 3883–3896.
Van Lith, Y., Vasconcelos, C., Warthmann, R., Martins, J.C.F., McKenzie, J.A., 2002. Bacterial sulfate reduction and salinity: two controls on dolomite precipitation in Lagoa Vermelha and Brejo do Espinho (Brazil). Hydrobiologia 485, 35–49.
Van Lith, Y., Warthmann, R., Vasconcelos, C., McKenzie, J.A., 2003a. Microbial fossilization in carbonate sediments: a result of the bacterial surface involvement in dolomite precipitation. Sedimentology 50, 237–245.
Van Lith, Y., Warthmann, R., Vasconcelos, C., McKenzie, J.A., 2003b. Sulphate-reducing bacteria induce low-temperature Ca-dolomite and high Mg-calcite formation. Geobiology 1, 71–79.
Vasconcelos, C., McKenzie, J.A., 1997. Microbial mediation of modern dolomite precipitation and diagenesis under anoxic conditions (Lagoa Vermelha, Rio De Janeiro, Brazil). J. Sediment. Res. 67, 378–390.
Vasconcelos, C., McKenzie, J.A., 2008. Dolomite as a biomineral and possible implications. Rev. Soc. Esp. Mineral. 9, 21–22.
Vasconcelos, C., McKenzie, J.A., Bernasconi, S., Grujic, D., Tien, A.J., 1995. Microbial mediation as a possible mechanism for natural dolomite formation at low temperatures. Nature 377, 220–222.
Warren, J., 2000. Dolomite: occurrence, evolution and economically important associations. Earth Sci. Rev. 52, 1–81.
Warthmann, R., Van Lith, Y., Vasconcelos, C., McKenzie, J.A., Karpoff, A.M., 2000. Bacterially induced dolomite precipitation in anoxic culture experiments. Geology 28, 1091–1094.
Williams, A.H., Walkden, G.M., 2002. Late Quaternary highstand deposits of the southern Arabian Gulf: a record of sea-level and climate change. In: Clift, P.D., Kroon, D., Gaedicke, C., Craig, J. (Eds.), Geological Society Special Publication, London 195, pp. 371–386.
Wimpenny, J., Colla, C.A., Yin, Q.-Z., Rustad, J.R., Casey, W.H., 2014a. Investigation the behaviour of Mg isotopes during the formation of clay minerals. Geochim. Cosmochim. Acta 182, 178–194.
Wimpenny, J., Yin, Q.-Z., Tollstrup, D., 2014b. Using Mg isotope ratios to trace Cenozoic weathering changes: a case study from the Chinese loess plateau. Chem. Geol. 376, 31–43.
Wood, W.W., Sanford, W.E., Al Habshi, A.R.S., 2002. Source of solutes to the coastal sabkha of Abu Dhabi. Geol. Soc. Am. Bull. 114, 259–268.
Wright, D.T., 1997. An organogenic origin for widespread dolomite in the Cambrian Eilean Dubh Formation, northwestern Scotland. J. Sediment. Res. 67, 54–64.
Wright, D.T., Wacey, D., 2005. Precipitation of dolomite using sulphate-reducing bacteria from the Coorong Region, South Australia: significance and implications. Sedimentology 52, 987–1008.
Young, E.D., Galy, A., 2004. The isotope geochemistry and cosmochemistry of magnesium. Rev. Mineral. Geochem. 55, 197–230.